COMMUNICATION

ADVANCED
MATERIALS
www.advmat.d

Check for
updates

Canonic-Like HER Activity of $Cr_{1-x}Mo_xB_2$ Solid Solution: Overpowering Pt/C at High Current Density

*Hyounmyung Park, Eunsoo Lee, Ming Lei, Hyunkeun Joo, Sinisa Coh, and Boniface P. T. Fokwa**

Abstract transition metal borides are emerging as substitute electrochemical hydrogen evolution reaction (HER) catalysts for noble metals. Herein, an unusual canonic-like behavior of the *c* lattice parameter in the AlB_2-type solid solution $Cr_{1-x}Mo_xB_2$ (x = 0, 0.25, 0.4, 0.5, 0.6, 0.75, 1) and its direct correlation to the HER activity in 0.5 M H_2SO_4 solution are reported. The activity increases with increasing *x*, reaching its maximum at x = 0.6 before decreasing again. At high current densities, $Cr_{0.4}Mo_{0.6}B_2$ outperforms Pt/C, as it needs 180 mV less overpotential to drive an 800 mA cm^{-2} current density. $Cr_{0.4}Mo_{0.6}B_2$ has excellent long-term stability and durability showing no significant activity loss after 5000 cycles and 25 h of operation in acid. First-principles calculations have correctly reproduced the nonlinear dependence of the *c* lattice parameter and have shown that the mixed metal/B layers, such as (110), promote hydrogen evolution more efficiently for x = 0.6, supporting the experimental results.

Hydrogen is considered as one of the most promising energy carriers because of its clean, renewable, and abundant nature.[1] Among various methods to produce hydrogen, electrochemical water splitting through hydrogen evolution reaction (HER) is highly attractive since it is efficient, sustainable, and environmentally friendly.[2] In water electrolysis, to efficiently attain hydrogen and reduce the overpotential, electrocatalysts play vital roles. To date, Pt group noble metals are considered as benchmark HER electrocatalysts showing extremely low

overpotential. Unfortunately, their low abundance and high price limit their large-scale application,[3] thus developing earth-abundant and high-performance HER electrocatalysts is inevitable.[4]

In the last few decades, non-noble metal electrocatalysts including oxides and sulfides,[5] nitrides,[6] phosphide,[7] carbides,[8] selenides,[9] chalcogenide solid solutions, and alloys[10] have shown remarkable HER activity.

Recently, transition metal borides such as Mo–B (bulk, nanoscale),[11–14] MoAlB (bulk),[15] Co-B (amorphous),[16] Ni–B (amorphous, nanoscale),[17] Co–Ni–B (amorphous),[18] FeB_2 (nanoscale),[19] and VB_2 (nanoscale)[20] have been considered as promising HER electrocatalysts due to their abundance, low cost, and their outstanding HER activity and stability both in acidic and alkaline solutions. Among these borides, those containing the flat (graphene-like) boron layer in their crystal structures such as MoB_2, FeB_2, and VB_2 have shown the highest HER performance.

Chromium is in the same group of the periodic table as molybdenum and tungsten and so they have some similar chemical properties such as building similar compositions with boron. However, they also have some differences: Cr is an antiferromagnetic element and can induce magnetism in metallic systems, for example, CrB_2 is also an antiferromagnetic material[21] while the corresponding molybdenum and tungsten dioborides are non-magnetic. Furthermore, CrB_2 and the AlB_2-type modification of MoB_2 have the same structure, containing flat graphene-like boron layers, while in WB_2, 50% of the boron layers are puckered. Interestingly, our recent experimental and density functional theory (DFT) HER studies have shown that the puckered (chair-like) boron layers are far less active than the flat boron layers,[13] making AlB_2-type MoB_2 a better catalyst than WB_2 even though elemental W has significantly higher activity than elemental Mo.[22] These findings suggested that a W-doped MoB_2 may have even better activity than MoB_2. Indeed, our experimental and DFT studies of $Mo_{1-x}W_xB_2$ (x < 0.4) solid solution have confirmed this hypothesis and have provided the best high current density HER boride electrocatalyst, $Mo_{0.7}W_{0.3}B_2$, to date.[22] DFT calculations have ascribed the excellent high current density behavior to tungsten, as it promotes hydrogen generation by facilitating bonding between nearby hydrogen atoms adsorbed on the boron layer. Consequently, a W-richer $Mo_{1-x}W_xB_2$ phase (x > 0.5) may have been an even better

Dr. H. Park, E. Lee, M. Lei, H. Joo, Prof. B. P. T. Fokwa
Department of Chemical and Environmental Engineering
University of California, Riverside
Riverside, CA 92521, USA
E-mail: bfokwa@ucr.edu
H. Park, E. Lee, Prof. B. P. T. Fokwa
Department of Chemistry
University of California, Riverside
Riverside, CA 92521, USA
Prof. S. Coh
Department of Mechanical Engineering and Materials Science
and Engineering Program
University of California, Riverside
Riverside, CA 92521, USA
Prof. B. P. T. Fokwa
Center for Catalysis
University of California, Riverside
Riverside, CA 92521, USA

electrocatalyst, but it could not be synthesized as the less HER-active WB_2-type structure was obtained instead. As mentioned above, CrB_2 and MoB_2 have the same AlB_2-type structure, thus a full solid solution range can be synthesized, enabling not only the HER study of Cr-based borides for the first time but also the impact of structure–activity relationships in such materials. Also, chromium is far more abundant and cheaper than molybdenum, making the $Cr_{1-x}Mo_xB_2$ solid solution even more attractive.

Herein, we report on the successful synthesis of the full solid solution $Cr_{1-x}Mo_xB_2$ ($x = 0$, 0.25, 0.4, 0.5, 0.6, 0.75, 1), which shows an intriguing canonic-like behavior of the c lattice parameter that perfectly correlates with its HER activity and enables a superior high current density behavior than Pt/C. In addition, we have applied DFT calculations to study the lattice parameter and the H-adsorption behaviors to support the experimental results.

The solid solution range of $Cr_{1-x}Mo_xB_2$ ($x = 0$, 0.25, 0.4, 0.5, 0.6, 0.75) was successfully synthesized by arc-melting according to the procedure given in the Supporting Information. As shown by Rietveld refinement plots (Figures S1 and S2, Supporting Information) of the powder X-ray diffraction (PXRD) patterns, all peaks are indexed in the AlB_2-type structure (Figure S3a, Supporting Information), indicating the high purity of the crystalline samples. The quantitative energy dispersive X-ray spectroscopy (EDS) analysis provides the Cr and Mo atomic percentages (Figure S4, Supporting Information), which were in good agreement with the loaded composition, thus further confirming the successful synthesis. In addition, the EDS mapping (Figure S4, Supporting Information) proved the uniform distribution of all elements (Cr, Mo, and B) in each sample. Also, a representative scanning electron microscopy (SEM) image of the $Cr_{0.4}Mo_{0.6}B_2$ electrode' surface (Figure S5, Supporting Information) shows a heterogeneous particle size distribution in the micrometer range, as expected from this polycrystalline sample. **Figure 1** shows the refined lattice parameters plotted as a function of the molybdenum content. The a-lattice parameter plot follows the expected linear behavior according to the Vegard's law, but the c-lattice parameter plot surprisingly shows a canonic-like behavior as it first increases with increasing x, reaching a maximum at 60 at% Mo ($Cr_{0.4}Mo_{0.6}B_2$) before decreasing. The available

lattice parameters for CrB_2, $Cr_{0.5}Mo_{0.5}B_2$ and MoB_2 from the ICSD database agree well with our refined values (Figure 1a,b).

In order to understand the unusual canonic-like behavior of the c-lattice parameter plot, we have carried out density functional theory (DFT) calculations (see Supporting Information for details) using non-spin-polarized (nsp, non-magnetic) and spin polarized (sp, magnetic) models for $Cr_{1-x}Mo_xB_2$ ($x = 0$, 1/3, 1/2, 2/3, 3/4, 4/5 1). The sp models are the ground states (most energetically stable states) except for MoB_2 that is non-magnetic. The reported antiferromagnetic state of CrB_2 was confirmed,[21] and used as basis for the AFM models of unreported $Cr_{1-x}Mo_xB_2$ ($x = 1/3$, 1/2, 2/3, 3/4, 4/5). This basic AFM model has correctly reproduced the nonlinear behavior of the c-lattice parameter plot (Figure 1c), while the nsp calculations show a linear behavior (Figure 1c) instead.

To analyze the surface chemical composition and electronic state of $Cr_{1-x}Mo_xB_2$ ($x = 0$, 0.25, 0.4, 0.5, 0.6, 0.75, 1), X-ray photoelectron spectroscopy (XPS) was performed (**Figure 2**; Figure S6, Tables S2 and S3, Supporting Information). As shown in Figure 2 and Figure S6, Supporting Information, the oxidation states of the chromium, molybdenum, and boron species present on the analyzed surfaces of all $Cr_{1-x}Mo_xB_2$ ($x = 0$, 0.25, 0.4, 0.5, 0.6, 0.75) phases are Cr^0, Mo^0, and B^0 from the metal boride as well as Cr^{3+}, Cr^{6+}, Mo^{3+}, Mo^{4+}, Mo^{6+}, and B^{3+} from the surface oxides of chromium,[23] molybdenum,[11,13] and boron.[24,25] The layer of surface oxide, which originates from exposing the materials in the air, is very thin as the metal boride underneath mostly dominates the spectra. XPS analysis of the material surface after HER measurements (Figure 2d,e) shows that the amount of oxide species on the surface has dramatically reduced, thus confirming the above finding that the oxide species readily dissolve in the acid and thus will not play any role in the HER activity (see next section). Measurements of the XPS surface compositions reveal comparable compositions to the bulk (EDS) within experimental error (Table S3 and Figure S4, Supporting Information).

The electrochemical HER activity of binary CrB_2 and ternary $Cr_{1-x}Mo_xB_2$ ($x = 0.25$, 0.4, 0.5, 0.6, 0.75) is studied here for the first time, while MoB_2 was reported previously as the best HER catalyst in acidic solutions among non-noble metal binary borides.[12,13,22] Our measurements were carried out using the
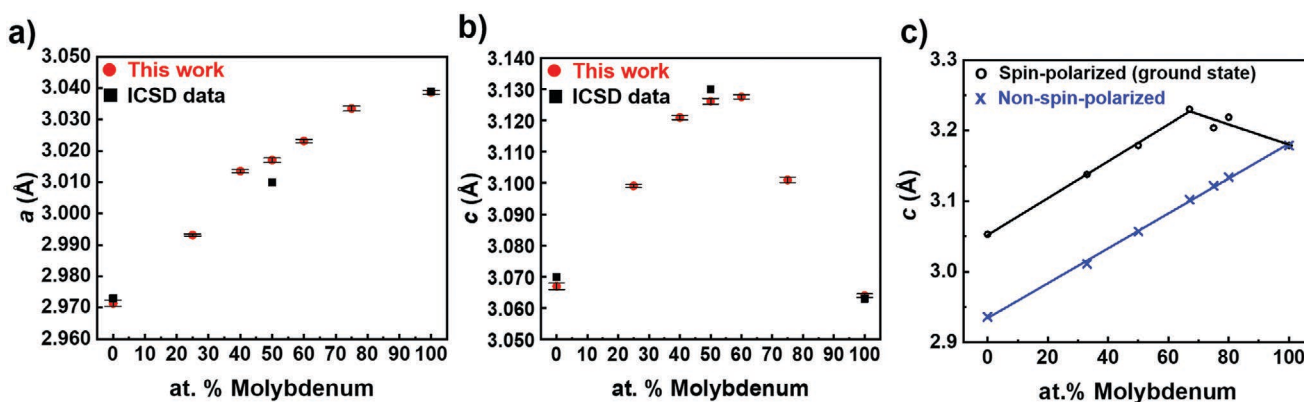

Figure 1. a,b) Plots of the refined lattice parameters from powder X-ray diffraction data of $Cr_{1-x}Mo_xB_2$ as a function of the molybdenum content. The black squares represent the reported ICSD data. c) Predicted lattice parameters from spin-polarized and non-spin-polarized DFT calculations. Lines are just a guide for the eyes.
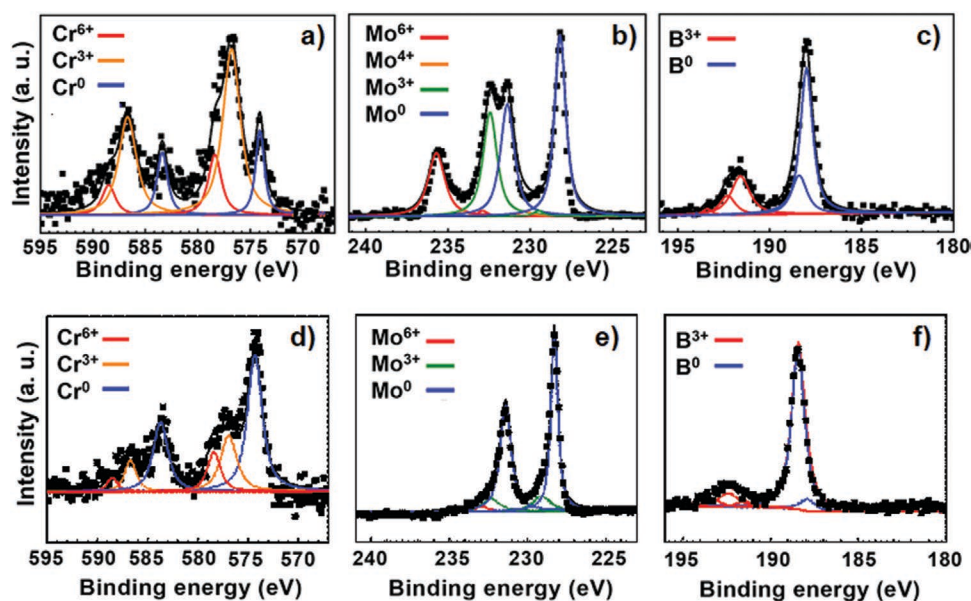
**ADVANCED
SCIENCE NEWS**

www.advancedsciencenews.com

**ADVANCED
MATERIALS**

www.advmat.de

Figure 2. a–f) X-ray photoelectron spectroscopy spectra of Cr 2p (a,d), Mo 3d (b,e), and B 1s (c,f) in $Cr_{0.4}Mo_{0.6}B_2$ before (top) and after (bottom) HER measurements. Experimental and fitting data are indicated as ■ and solid lines, respectively.

standard three electrodes system in acidic (0.5 M H_2SO_4) electrolyte at a scan rate of 5 mV s^{-1} with IR-drop compensation (**Figures 3**a; Figure S7a, Supporting Information). The working electrodes were prepared by attaching disc-shaped, arc-melted samples on copper sheets (see Supporting Information and the study by Park et al.[22] for more details).
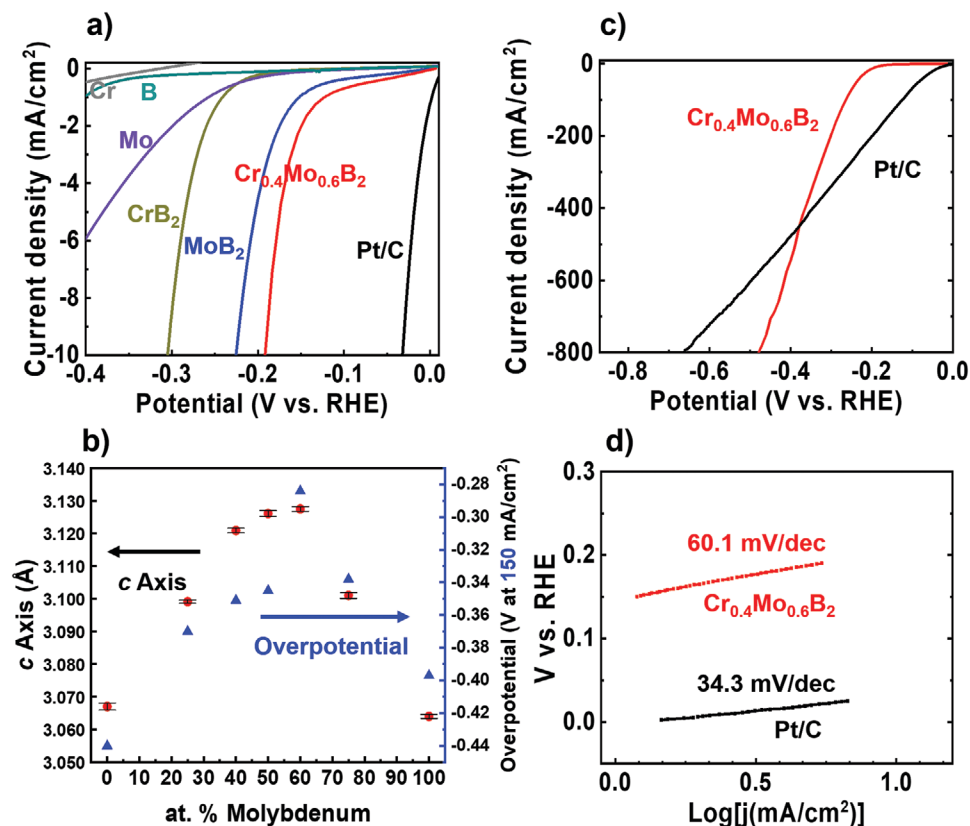

Figure 3. a) Linear sweep polarization curves of different materials recorded in 0.5 M H_2SO_4 (current density normalized with the electrode's geometric surface area). b) Plots of the lattice parameter c and the overpotential (at 150 mA cm^{-2} current density) as a function of molybdenum content. c) Linear sweep polarization curves showing the high current density behaviors of $Cr_{0.4}Mo_{0.6}B_2$ and 20% Pt/C. d) Tafel plots of $Cr_{0.4}Mo_{0.6}B_2$ and 20% Pt/C.

According to the polarization curves plotted on Figure 3a, Pt/C has the lowest overpotential of −32 mV to drive a current density of 10 mA cm^{-2} as expected,[26,27] while all elemental materials (B, Cr, and Mo) have very high overpotentials (Mo: −468 mV, B: −505 mV, and Cr: −628 mV) and are the least active. All borides are much more active than their individual components. MoB$_2$ is confirmed as a very active catalyst with an overpotential of −225 mV that is 80 mV lower than that of CrB$_2$ (−305 mV) at 10 mA cm^{-2}; however, this difference significantly decreases to only 45 mV at 150 mA cm^{-2} (Figure S7a, Supporting Information), indicating a greatly improved HER activity for CrB$_2$ at high current density. Nevertheless, the activity difference between these two binary catalysts is likely due to the much higher activity of elemental Mo if compared to elemental Cr (Figure 3a). This argument is further verified in the Cr$_{1-x}$Mo$_x$B$_2$ solid solution, the HER activity of which increases with increasing molybdenum content (x) reaching a maximum at $x = 0.6$ before decreasing (Figure S7c, Supporting Information). Interestingly, the best catalyst, Cr$_{0.4}$Mo$_{0.6}$B$_2$, has a 32 mV smaller overpotential (−193 mV at 10 mA cm^{-2}) than that of MoB$_2$. Even more impressive is the high current density performance of Cr$_{0.4}$Mo$_{0.6}$B$_2$, whose overpotential to drive 150 mA cm^{-2} current density is more than 100 mV smaller than that of MoB$_2$. In fact, all ternary Cr$_{1-x}$Mo$_x$B$_2$ compositions have smaller overpotentials at 150 mA cm^{-2} current density than MoB$_2$, and astonishingly a plot of overpotential as a function of molybdenum content follows the same canonic-like behavior as the c-lattice parameter (Figure 3b). This is a significant finding because it shows that variation of the lattice parameter can have a drastic influence on the HER activity of catalysts, thus hinting at the future design of more efficient catalysts by leveraging the structure–activity relationships in this and other structure types. It also shows that careful examination of crystal structures through structure–activity relationships in other HER catalyst classes (carbides, nitrides, phosphides, etc.) can be a useful tool to design next-generation electrocatalysts. While the effect of solid solution has been studied in the past and has achieved extraordinary results, for example in MoS$_{2(1-x)}$P$_x$,[10c] and CoS$_{2(1-x)}$Se$_x$,[10d] only linear dependencies of the lattice parameters were observed, contrary to the canonic-like behavior found in our work.

Interestingly, increasing the current density above the industrially relevant value of 300 mA cm^{-2}[28] not only further increases the overpotential gap between MoB$_2$ and Cr$_{0.4}$Mo$_{0.6}$B$_2$, but it also leads to a much better performance of Cr$_{0.4}$Mo$_{0.6}$B$_2$ than 20% Pt/C as it needs 180 mV less overpotential to drive an 800 mA cm^{-2} current density (Figure 3c), a further proof of the remarkable performance of this material at high current density.

The HER catalytic mechanism is usually revealed by Tafel plot. Typically, there are three classical reactions that can be the rate-determining step (RDS): the Volmer reaction (electrochemical hydrogen ion adsorption, Tafel slope of ≈120 mV dec^{-1}), the Heyrovsky reaction (electrochemical desorption, Tafel slope of ≈40 mV dec^{-1}), and the Tafel reaction (chemical desorption, Tafel slope of ≈30 mV dec^{-1}). The first step of HER is the Volmer reaction, followed by either the Heyrovsky or the Tafel reaction.[29] The calculated Tafel slopes of all samples are given in Figure 3d and Figure S7b, Supporting Information. The Tafel slope of Pt/C (34.3 mV dec^{-1}) is the lowest of all, confirming its faster kinetics and the Tafel reaction as the RDS. All the borides' Tafel slopes range between 60.1 and 90.3 mV dec^{-1}, thus these values do not match any theoretical Tafel slope and it is difficult to determine the RDS using Tafel analysis because of the reaction complexity of bulk HER catalyst. However, Cr$_{0.4}$Mo$_{0.6}$B$_2$ exhibits the lowest Tafel slope, demonstrating a much faster and efficient process of HER than for all other boride compositions.

The electrochemically active surface area (ECSA) of the newly studied metal borides CrB$_2$ and Cr$_{1-x}$Mo$_x$B$_2$ ($x = 0.25$, 0.4, 0.5, 0.6, 0.75) was estimated by the double layer capacitance (C_{dl}) through cyclic voltammetry (CV) at various scan rates (0.05–0.15 V vs reversible hydrogen electrode).[30] In accordance with the obtained C_{dl} values (Figure S8, Supporting Information), Cr$_{0.4}$Mo$_{0.6}$B$_2$ has the highest ECSA (or highest number of active sites) of all binary and ternary borides, thereby further confirming the higher performance of Cr$_{0.4}$Mo$_{0.6}$B$_2$. In addition, the electrochemical impedance spectroscopy (EIS) measurements (Figure S9, Supporting Information) show that Cr$_{0.4}$Mo$_{0.6}$B$_2$ has the smallest electron transfer resistance and the EIS trend within the solid solution is in good agreement with the HER activity trend.

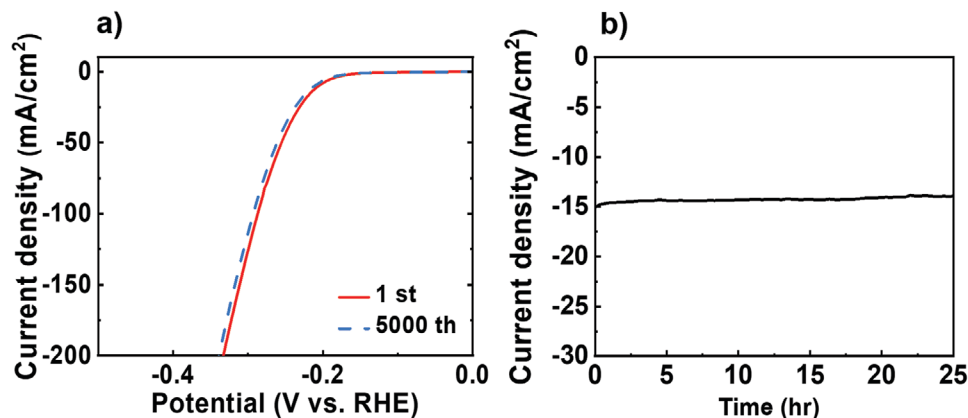**Figure 4.** a) HER stability measurement of Cr$_{0.4}$Mo$_{0.6}$B$_2$ at the 1st and 5000th cycles with a scan rate of 100 mV s^{-1} in 0.5 M H$_2$SO$_4$. b) Chronoamperometry curve of Cr$_{0.4}$Mo$_{0.6}$B$_2$ for 25 h.
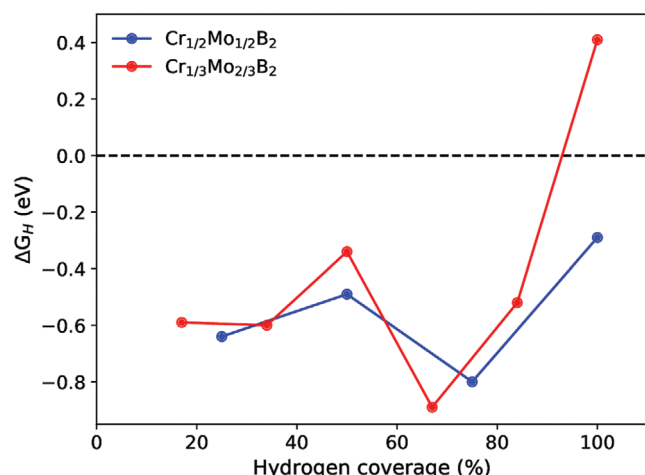
Figure 5. Gibbs free energy (ΔG_H) for H adsorption on the (110) surfaces of $Cr_{1-x}Mo_xB_2$ ($x = 1/2, 2/3$) plotted as a function of hydrogen coverage.

The long-term durability test of $Cr_{0.4}Mo_{0.6}B_2$ was evaluated by potential cycling in 0.5 M H_2SO_4. As shown in **Figure 4**a, no appreciable activity loss occurred after 5000 cycles. In addition, the chronoamperometry curve for $Cr_{0.4}Mo_{0.6}B_2$ indicates that the current density of $Cr_{0.4}Mo_{0.6}B_2$ is maintained at a constant value with a negligible loss after 25 h operation, revealing the excellent long-term electrochemical stability of $Cr_{0.4}Mo_{0.6}B_2$ (Figure 4b).

It has been demonstrated, through calculations of the Gibbs free energy for hydrogen evolution (ΔG_H), that the flat graphene-like boron layer in all studied AlB_2-type boride electrocatalysts (MoB_2,[13] FeB_2,[19] VB_2,[20] $Mo_{0.7}W_{0.3}B_2$[25]) is the most HER-active surface. For the current calculations, we will, therefore, focus on understanding the role of the Cr/Mo ratio in achieving the best catalyst in the $Cr_{1-x}Mo_xB_2$ ($x = 0, 0.25, 0.4, 0.5, 0.6, 0.75$; AlB_2-type) solid solution. We have, therefore, chosen $Cr_{1-x}Mo_xB_2$ ($x = 1/2, 2/3$) as representatives since both compositions are the closest to the best catalyst, $Cr_{0.4}Mo_{0.6}B_2$. Furthermore, we have recently shown that the mixed metal/boron (110) surface is not only another active surface in Mo-based AlB_2-type borides, it is also a good model surface to study the H-adsorption behavior in bimetallic AlB_2-type borides.[25] The calculated ΔG_H is plotted in **Figure 5** as a function of H-coverage on the mixed Mo/Cr (110) surface of $Cr_{1-x}Mo_xB_2$ ($x = 1/2, 2/3$). At all H-coverages, ΔG_H of $Cr_{1/2}Mo_{1/2}B_2$ never reaches zero, while it reaches zero between 85% and 90% H-coverage for $Cr_{1/3}Mo_{2/3}B_2$, indicating that the (110) layer performs much better in the latter composition, thus corroborating experimental findings. Furthermore, in previous Mo-based borides, the ΔG_H plot for (110) surface crossed zero below 60%,[25] a value that is much lower than that of $Cr_{1/3}Mo_{2/3}B_2$, indicating a better performance of the latter at high H-coverages, hence a better high current density catalyst, in agreement with experimental results.

In summary, single-phase bulk solid solution $Cr_{1-x}Mo_xB_2$ ($x = 0, 0.25, 0.4, 0.5, 0.6, 0.75$, AlB_2-type structure) has been successfully synthesized by arc melting and fully characterized for the first time. We found that the ternary compositions have higher HER activity than the binary ones and that the HER activity of the solid solution follows the same canonic-like behavior as the c lattice parameter. DFT calculations could reproduce the behavior of the c lattice

parameter and demonstrate that the mixed metal/B (110) layer promotes hydrogen evolution more efficiently for $x = 0.6$. Among the ternary $Cr_{1-x}Mo_xB_2$ electrochemical catalyst, $Cr_{0.4}Mo_{0.6}B_2$ exhibits the highest HER activity and has even higher HER activity than Pt/C at high current densities in acidic solution. $Cr_{0.4}Mo_{0.6}B_2$ has excellent long-term stability showing no significant HER activity loss after 5000 cycles and 25 h of operation in an acid electrolyte.

Supporting Information

Supporting Information is available from the Wiley Online Library or from the author.

Conflict of Interest

The authors declare no conflict of interest.

[1] a) J. A. Turner, *Science* **2004**, *305*, 972; b) N. S. Lewis, D. G. Nocera, *Proc. Natl. Acad. Sci. USA* **2006**, *103*, 15729; c) M. Dresselhaus, I. Thomas, *Nature* **2001**, *414*, 332.

[2] a) J. Wang, W. Cui, Q. Liu, Z. Xing, A. M. Asiri, X. Sun, *Adv. Mater.* **2016**, *28*, 215; b) A. B. Laursen, S. Kegnæs, S. Dahl, I. Chorkendorff, *Energy Environ. Sci.* **2012**, *5*, 5577.

[3] a) M. S. Faber, S. Jin, *Energy Environ. Sci.* **2014**, *7*, 3519; b) Y. Jiao, Y. Zheng, M. Jaroniec, S. Z. Qiao, *Chem. Soc. Rev.* **2015**, *44*, 2060; c) C. G. Morales-Guio, L. A. Stern, X. Hu, *Chem. Soc. Rev.* **2014**, *43*, 6555.

[4] a) Y. Shi, B. Zhang, *Chem. Soc. Rev.* **2016**, *45*, 1529; b) Q. Lu, Y. Yu, Q. Ma, B. Chen, H. Zhang, *Adv. Mater.* **2016**, *28*, 1917.

[5] a) T. F. Jaramillo, K. P. Jørgensen, J. Bonde, J. H. Nielsen, S. Horch, I. Chorkendorff, *Science* **2007**, *317*, 100; b) D.-Y. Wang, M. Gong, H. L. Chou, C.-J. Pan, H. A. Chen, Y. Wu, M. C. Lin, M. Guan, J. Yang, C. W. Chen, *J. Am. Chem. Soc.* **2015**, *137*, 1587; c) J. Staszak-Jirkovský, C. D. Malliakas, P. P. Lopes, N. Danilovic, S. S. Kota, K.-C. Chang, B. Genorio, D. Strmcnik, V. R. Stamenkovic, M. G. Kanatzidis, *Nat. Mater.* **2016**, *15*, 197; d) F. A. Garcés-Pineda, M. Blasco-Ahicart, D. Nieto-Castro, N. López, J. R. Galán-Mascarós, *Nat. Energy* **2019**, *4*, 519.

[6] a) W.-F. Chen, J. T. Muckerman, E. Fujita, *Chem. Commun.* **2013**, *49*, 8896; b) W. F. Chen, K. Sasaki, C. Ma, A. I. Frenkel, N. Marinkovic,

J. T. Muckerman, Y. Zhu, R. R. Adzic, *Angew. Chem., Int. Ed.* **2012**, *51*, 6131.

[7] a) X. Xiao, L. Tao, M. Li, X. Lv, D. Huang, X. Jiang, H. Pan, M. Wang, Y. Shen, *Chem. Sci.* **2018**, *9*, 1970; b) R. Zhang, X. Wang, S. Yu, T. Wen, X. Zhu, F. Yang, X. Sun, X. Wang, W. Hu, *Adv. Mater.* **2017**, *29*, 1605502; c) J. F. Callejas, J. M. McEnaney, C. G. Read, J. C. Crompton, A. J. Biacchi, E. J. Popczun, T. R. Gordon, N. S. Lewis, R. E. Schaak, *ACS Nano* **2014**, *8*, 11101; d) E. J. Popczun, J. R. McKone, C. G. Read, A. J. Biacchi, A. M. Wiltrout, N. S. Lewis, R. E. Schaak, *J. Am. Chem. Soc.* **2013**, *135*, 9267.

[8] a) R. Michalsky, Y. J. Zhang, A. A. Peterson, *ACS Catal.* **2014**, *4*, 1274; b) L. Liao, S. Wang, J. Xiao, X. Bian, Y. Zhang, M. D. Scanlon, X. Hu, Y. Tang, B. Liu, H. H. Girault, *Energy Environ. Sci.* **2014**, *7*, 387; c) W.-F. Chen, C.-H. Wang, K. Sasaki, N. Marinkovic, W. Xu, J. Muckerman, Y. Zhu, R. Adzic, *Energy Environ. Sci.* **2013**, *6*, 943; d) S. M. Schmuecker, D. Clouser, T. J. Kraus, B. M. Leonard, *Dalton Trans.* **2017**, *46*, 13524.

[9] a) D. Kong, H. Wang, J. J. Cha, M. Pasta, K. J. Koski, J. Yao, Y. Cui, *Nano Lett.* **2013**, *13*, 1341; b) K. Xu, F. Wang, Z. Wang, X. Zhan, Q. Wang, Z. Cheng, M. Safdar, J. He, *ACS Nano* **2014**, *8*, 8468; c) X. Wang, Y. Chen, B. Zheng, F. Qi, J. He, P. Li, W. Zhang, *Electrochim. Acta* **2016**, *222*, 1293.

[10] a) S. E. Fosdick, S. P. Berglund, C. B. Mullins, R. M. Crooks, *ACS Catal.* **2014**, *4*, 1332; b) H. Lv, Z. Xi, Z. Chen, S. Guo, Y. Yu, W. Zhu, Q. Li, X. Zhang, M. Pan, G. Lu, *J. Am. Chem. Soc.* **2015**, *137*, 5859; c) R. Ye, P. del Angel-Vicente, Y. Liu, M. J. Arellano-Jimenez, Z. Peng, T. Wang, Y. Li, B. I. Yakobson, S.-H. Wei, M. J. Yacaman, J. M. Tour, *Adv. Mater.* **2016**, *28*, 1427; d) L. Fang, W. Li, Y. Guan, Y. Feng, H. Zhang, S. Wang, Y. Wang, *Adv. Funct. Mater.* **2017**, *727*, 1701008.

[11] H. Vrubel, X. Hu, *Angew. Chem., Int. Ed.* **2012**, *51*, 12703.

[12] a) H. Park, A. Encinas, J. P. Scheifers, Y. Zhang, B. P. Fokwa, *Angew. Chem., Int. Ed.* **2017**, *56*, 5575; b) P. R. Jothi, Y. Zhang, J. P. Scheifers, H. Park, B. P. Fokwa, *Sustainable Energy Fuels* **2017**, *1*, 1928.

[13] H. Park, Y. Zhang, J. P. Scheifers, P. R. Jothi, A. Encinas, B. P. Fokwa, *J. Am. Chem. Soc.* **2017**, *139*, 12915.

[14] X. Wang, G. Tai, Z. Wu, T. Hu, R. Wang, *J. Mater. Chem. A* **2017**, *5*, 23471.

[15] L. T. Alameda, C. F. Holder, J. L. Fenton, R. E. Schaak, *Chem. Mater.* **2017**, *29*, 8953.

[16] a) S. Gupta, N. Patel, A. Miotello, D. Kothari, *J. Power Sources* **2015**, *279*, 620; b) J. Masa, P. Weide, D. Peeters, I. Sinev, W. Xia, Z. Sun, C. Somsen, M. Muhler, W. Schuhmann, *Adv. Energy Mater.* **2016**, *6*, 1502313; c) Z. Chen, Q. Kang, G. Cao, N. Xu, H. Dai, P. Wang, *Int. J. Hydrogen Energy* **2018**, *43*, 6076.

[17] a) P. Los, A. Lasia, *J. Electroanal. Chem.* **1992**, *333*, 115; b) M. Zeng, H. Wang, C. Zhao, J. Wei, K. Qi, W. Wang, X. Bai, *ChemCatChem* **2016**, *8*, 708.

[18] N. Xu, G. Cao, Z. Chen, Q. Kang, H. Dai, P. Wang, *J. Mater. Chem. A* **2017**, *5*, 12379.

[19] H. Li, P. Wen, Q. Li, C. Dun, J. Xing, C. Lu, S. Adhikari, L. Jiang, D. L. Carroll, S. M. Geyer, *Adv. Energy Mater.* **2017**, *7*, 1700513.

[20] P. R. Jothi, Y. Zhang, K. Yubuta, D. Culver, M. P. Conley, B. P. Fokwa, *ACS Appl. Energy Mater.* **2019**, *2*, 176.

[21] R. Barnes, R. Creel, *Phys. Lett. A* **1969**, *29*, 203.

[22] H. Park, Y. Zhang, E. Lee, P. Shankhari, B. P. Fokwa, *ChemSusChem* **2019**, *12*, 3726.

[23] a) J. Sainio, M. Aronniemi, O. Pakarinen, K. Kauraala, S. Airaksinen, O. Krause, J. Lahtinen, *Appl. Surf. Sci.* **2005**, *252*, 1076; b) N. Fiol, C. Escudero, I. Villaescusa, *Bioresour. Technol.* **2008**, *99*, 5030.

[24] B. R. Terlan, A. A. Levin, F. Börrnert, F. Simon, M. Oschatz, M. Schmidt, R. Cardoso-Gil, T. Lorenz, I. A. Baburin, J.-O. Joswig, *Chem. Mater.* **2015**, *27*, 5106.

[25] Y. Wang, M. Trenary, *Chem. Mater.* **1993**, *5*, 199.

[26] J. Tian, Q. Liu, A. M. Asiri, X. Sun, *J. Am. Chem. Soc.* **2014**, *136*, 7587.

[27] a) C. Wang, T. Wang, J. Liu, Y. Zhou, D. Yu, F. Han, Q. Li, J. Chen, Y. Huang, *Energy Environ. Sci.* **2018**, *11*, 2467; b) C. Wang, T. Wang, J. Liu, Y. Zhou, D. Yu, J.-K. Chang, F. Han, Q. Li, J.-T. Chen, Y. Huang, *Energy Environ. Sci.* **2018**, *11*, 2467.

[28] K. Zeng, D. Zhang, *Prog. Energy Combust. Sci.* **2010**, *36*, 307.

[29] a) D. Y. Chung, S. K. Park, Y. H. Chung, S. H. Yu, D. H. Lim, N. Jung, H. C. Ham, H. Y. Park, Y. Piao, S. J. Yoo, *Nanoscale* **2014**, *6*, 2131; b) Y. J. Tang, M. R. Gao, C. H. Liu, S. L. Li, H. L. Jiang, Y. Q. Lan, M. Han, S. H. Yu, *Angew. Chem., Int. Ed.* **2015**, *54*, 12928; c) A. Kahyarian, B. Brown, S. Nesic, *J. Electrochem. Soc.* **2017**, *164*, H365.

[30] a) J. D. Benck, Z. Chen, L. Y. Kuritzky, A. J. Forman, T. F. Jaramillo, *ACS Catal.* **2012**, *2*, 1916; b) M. A. Lukowski, A. S. Daniel, F. Meng, A. Forticaux, L. Li, S. Jin, *J. Am. Chem. Soc.* **2013**, *135*, 10274.